Application of PS-ADI-MRTD Method in Frequency Selective Surface Analysis

Yawen Liu and Pin Zhang

PLA University of Army Engineering, Nanjing, 210007, China
liuyawen1111@163.com, pinzhangthree@sina.com

Abstract ─ In this paper, a novel periodic spectral alternating direction implicit multi-resolution time domain (PS-ADI-MRTD) method is proposed for solving periodic structures. The algorithm for inversion of the block periodic tri-diagonal matrices is presented. A typical example is given to validate the effectiveness of the proposed algorithm, and the numerical results also show that the proposed algorithm can save more computation time than the traditional MRTD method. Furthermore, the PS-ADI-MRTD method is applied to analyze the electromagnetic scattering characteristics of two types frequency selective surface (FSS) structures.

Index Terms ─ Alternating Direction Implicit (ADI), Frequency Selective Surface (FSS), Multi-Resolution Time Domain (MRTD), spectral technique.

I. INTRODUCTION

The Multi-Resolution Time-Domain (MRTD) technique was first proposed by Krumpholz and Katehi [1-2]. Although with a high linear dispersion performance [3-5], the MRTD method has a major disadvantage that the time stability condition is stricter than FDTD [2], which limits the computational efficiency of the MRTD method. In 2001, Chen [6] proposed the ADI-MRTD method, which is unconditionally stable, that is, the choice of time step is not limited to the size of space interval.

In computational electromagnetics, there are various periodic structures, such as gratings, photonic bandgaps (PBG), frequency selective surfaces (FSS) and phased antenna arrays. And notable progress on the engineering applications of periodic structures has been achieved at the same time [7-13]. In this paper, the spectral technique [11-13] is applied to ADI-MRTD method, resulting in the periodic spectrum ADI-MRTD (PS-ADI-MRTD) algorithm. With the advantages of highly-linear dispersion performance and the CTW wave, it is suitable for calculating the periodic structures with high efficiency and oblique incidence. Moreover, a block periodic tridiagonal matrix inversion algorithm is presented. The scattering analysis of square thin plate arrays verifies the effectiveness and effectiveness of this method, and the numerical simulation shows that PS-ADI-MRTD has a good performance in saving computing time.

At the end, the PS-ADI-MRTD method is used to analyze the frequency scattering characteristics of a patch-type frequency selective surface and an aperture-type frequency selective surface, and the influence of incident angle and array arrangement on their dispersion characteristics is also discussed.

II. THE PROPOSED PS-ADI-MRTD ALGORITHM

The basic equations form of the PS-ADI-MRTD is similar to that of the ADI-MRTD [6]. In the PS-ADI-MRTD method, the Maxwell's equations are divided into two sub-steps, $(n+1/2)$ th and $(n+1)$ th step. Taking E_x and H_z as example, in the $(n+1/2)$ th sub-step, the following difference updating equations can be obtained as:

$$E_x^{n+\frac{1}{2}}\left(i+\tfrac{1}{2},j,k\right)=CA_x\left(i+\tfrac{1}{2},j,k\right)E_x^{n}\left(i+\tfrac{1}{2},j,k\right)+CB_x\left(i+\tfrac{1}{2},j,k\right)\left(\begin{array}{l}\frac{1}{\Delta y}\sum_l a(l)H_z^{n+\frac{1}{2}}\left(i+\tfrac{1}{2},j+l+\tfrac{1}{2},k\right)\\ -\frac{1}{\Delta z}\sum_l a(l)H_y^{n}\left(i+\tfrac{1}{2},j,k+l+\tfrac{1}{2}\right)\end{array}\right), \tag{1}$$

$$H_z^{n+\frac{1}{2}}\left(i+\tfrac{1}{2},j+\tfrac{1}{2},k\right)=CP_z\left(i+\tfrac{1}{2},j+\tfrac{1}{2},k\right)H_z^{n}\left(i+\tfrac{1}{2},j+\tfrac{1}{2},k\right)+CQ_z\left(i+\tfrac{1}{2},j+\tfrac{1}{2},k\right)\left(\begin{array}{l}\frac{1}{\Delta y}\sum_l a(l)E_x^{n+\frac{1}{2}}\left(i+\tfrac{1}{2},j+l+1,k\right)\\ -\frac{1}{\Delta x}\sum_l a(l)E_y^{n}\left(i+l+1,j+\tfrac{1}{2},k\right)\end{array}\right). \tag{2}$$

In the $(n+1)$ th sub-step, the difference updating equations can be obtained as:

Submitted On: April 14, 2019
Accepted On: April 12, 2020

$$E_x^{n+1}\left(i+\tfrac{1}{2},j,k\right)=CA_x\left(i+\tfrac{1}{2},j,k\right)E_x^{n+\frac{1}{2}}\left(i+\tfrac{1}{2},j,k\right)$$
$$+CB_x\left(i+\tfrac{1}{2},j,k\right)\left(\begin{array}{l}\dfrac{1}{\Delta y}\sum_l a(l)H_z^{n+\frac{1}{2}}\left(i+\tfrac{1}{2},j+l+\tfrac{1}{2},k\right)\\ -\dfrac{1}{\Delta z}\sum_l a(l)H_y^{n+1}\left(i+\tfrac{1}{2},j,k+l+\tfrac{1}{2}\right)\end{array}\right), \tag{3}$$

$$H_z^{n+1}\left(i+\tfrac{1}{2},j+\tfrac{1}{2},k\right)$$
$$=CP_z\left(i+\tfrac{1}{2},j+\tfrac{1}{2},k\right)H_z^{n+\frac{1}{2}}\left(i+\tfrac{1}{2},j+\tfrac{1}{2},k\right)$$
$$+CQ_z\left(i+\tfrac{1}{2},j+\tfrac{1}{2},k\right)\left(\begin{array}{l}\dfrac{1}{\Delta y}\sum_l a(l)E_x^{n+\frac{1}{2}}\left(i+\tfrac{1}{2},j+l+1,k\right)\\ -\dfrac{1}{\Delta x}\sum_l a(l)E_y^{n+1}\left(i+l+1,j+\tfrac{1}{2},k\right)\end{array}\right), \tag{4}$$

where

$$\left.\begin{array}{l}CA_x\left(i+\dfrac{1}{2},j,k\right)=\dfrac{4\varepsilon-\sigma\Delta t}{4\varepsilon+\sigma\Delta t}\\ CB_x\left(i+\dfrac{1}{2},j,k\right)=\dfrac{2\Delta t}{4\varepsilon+\sigma\Delta t}\\ CP_z\left(i+\dfrac{1}{2},j+\dfrac{1}{2},k\right)=\dfrac{4\mu-\sigma_m\Delta t}{4\mu+\sigma_m\Delta t}\\ CQ_z\left(i+\dfrac{1}{2},j+\dfrac{1}{2},k\right)=\dfrac{2\Delta t}{4\mu+\sigma_m\Delta t}\end{array}\right\}. \tag{5}$$

The coefficients $a(l)$ for $0\le l\le 2$ have been tabulated in [3], and the coefficients $a(l)$ for $l<0$ are given by the symmetry relation $a(-1-l)=-a(l)$:

$$E_x^{n+\frac{1}{2}}\left(i+\tfrac{1}{2},j,k\right)-\frac{CB_x}{\Delta y^2}$$
$$\times\sum_l a(l)CQ_z\sum_m a(m)E_x^{n+\frac{1}{2}}\left(i+\tfrac{1}{2},j+l+m+1,k\right)$$
$$=CA_xE_x^{n}\left(i+\tfrac{1}{2},j,k\right)+CB_x\times$$
$$\left(\begin{array}{l}\dfrac{1}{\Delta y}\sum_l a(l)CP_zH_z^{n}\left(i+\tfrac{1}{2},j+l+\tfrac{1}{2},k\right)\\ -\dfrac{1}{\Delta z}\sum_l a(l)H_y^{n}\left(i+\tfrac{1}{2},j,k+l+\tfrac{1}{2}\right)\\ -\dfrac{1}{\Delta x\Delta y}\sum_l a(l)CQ_z\sum_m a(m)E_y^{n}\left(i+m+1,j+l+\tfrac{1}{2},k\right)\end{array}\right). \tag{6}$$

Observing Eq. (1), we can see that Eq. (1) cannot be solved directly because both sides of Eq. (1) contain unknown components. It needs the unknown $H_z^{n+1/2}$ component to compute the $E_x^{n+1/2}$ component, so we can substitute Eq. (2) into Eq. (1), and the equation for $E_x^{n+1/2}$ can be obtained as Eq. (6) by proper rearrangement.

In free space, the above formula can be simplified as:

$$E_x^{n+\frac{1}{2}}\left(i+\tfrac{1}{2},j,k\right)-\frac{\Delta t^2}{4\varepsilon\mu\Delta y^2}\times$$
$$\sum_l a(l)\sum_m a(m)E_x^{n+\frac{1}{2}}\left(i+\tfrac{1}{2},j+l+m+1,k\right)$$
$$=E_x^{n}\left(i+\tfrac{1}{2},j,k\right)+$$
$$\frac{\Delta t}{2\varepsilon}\left(\begin{array}{l}\dfrac{1}{\Delta y}\sum_l a(l)H_z^{n}\left(i+\tfrac{1}{2},j+l+\tfrac{1}{2},k\right)\\ -\dfrac{1}{\Delta z}\sum_l a(l)H_y^{n}\left(i+\tfrac{1}{2},j,k+l+\tfrac{1}{2}\right)\\ -\dfrac{\Delta t}{2\mu\Delta x\Delta y}\sum_l a(l)\sum_m a(m)E_y^{n}\left(i+m+1,j+l+\tfrac{1}{2},k\right)\end{array}\right). \tag{7}$$

Similarly, we can obtain the equation for electric fields at the (n+1)th step:

$$E_x^{n+1}\left(i+\tfrac{1}{2},j,k\right)-$$
$$\frac{\Delta t^2}{4\varepsilon\mu\Delta z^2}\sum_l a(l)\sum_m a(m)E_x^{n+1}\left(i+\tfrac{1}{2},j,k+l+m+1\right)$$
$$=E_x^{n+\frac{1}{2}}\left(i+\tfrac{1}{2},j,k\right)+$$
$$\frac{\Delta t}{2\varepsilon}\left(\begin{array}{l}\dfrac{1}{\Delta y}\sum_l a(l)H_z^{n+\frac{1}{2}}\left(i+\tfrac{1}{2},j+l+\tfrac{1}{2},k\right)\\ -\dfrac{1}{\Delta z}\sum_l a(l)H_y^{n+\frac{1}{2}}\left(i+\tfrac{1}{2},j,k+l+\tfrac{1}{2}\right)\\ -\dfrac{\Delta t}{2\mu\Delta x\Delta z}\sum_l a(l)\sum_m a(m)E_z^{n+\frac{1}{2}}\left(i+m+1,j,k+l+\tfrac{1}{2}\right)\end{array}\right). \tag{8}$$

Taking Eq. (6) as example, the left side of Eq. (6) can be expressed as:

$$\begin{array}{l}A_j^eE_x^{n+\frac{1}{2}}\left(i+\tfrac{1}{2},j-5,k\right)+B_j^eE_x^{n+\frac{1}{2}}\left(i+\tfrac{1}{2},j-4,k\right)+\\ C_j^eE_x^{n+\frac{1}{2}}\left(i+\tfrac{1}{2},j-3,k\right)+D_j^eE_x^{n+\frac{1}{2}}\left(i+\tfrac{1}{2},j-2,k\right)+\\ E_j^eE_x^{n+\frac{1}{2}}\left(i+\tfrac{1}{2},j-1,k\right)+F_j^eE_x^{n+\frac{1}{2}}\left(i+\tfrac{1}{2},j,k\right)+\\ G_j^eE_x^{n+\frac{1}{2}}\left(i+\tfrac{1}{2},j+1,k\right)+H_j^eE_x^{n+\frac{1}{2}}\left(i+\tfrac{1}{2},j+2,k\right)+\\ I_j^eE_x^{n+\frac{1}{2}}\left(i+\tfrac{1}{2},j+3,k\right)+J_j^eE_x^{n+\frac{1}{2}}\left(i+\tfrac{1}{2},j+4,k\right)+\\ K_j^eE_x^{n+\frac{1}{2}}\left(i+\tfrac{1}{2},j+5,k\right)=L_j^e\end{array}, \tag{9}$$

where

$$\left.\begin{aligned}
&A_j^e=-\frac{a^2(-3)\Delta t^2}{4\varepsilon\mu\Delta y^2},\ B_j^e=-\frac{2a(-3)a(-2)\Delta t^2}{4\varepsilon\mu\Delta y^2}\\
&C_j^e=-\frac{\left[2a(-3)a(-1)+a^2(-2)\right]\Delta t^2}{4\varepsilon\mu\Delta y^2}\\
&D_j^e=-\frac{\left[2a(-3)a(0)+2a(-2)a(-1)\right]\Delta t^2}{4\varepsilon\mu\Delta y^2}\\
&E_j^e=-\frac{\left[2a(-3)a(1)+2a(-2)a(0)+a^2(-1)\right]\Delta t^2}{4\varepsilon\mu\Delta y^2}\\
&F_j^e=1-\frac{\left[2a(-3)a(2)+2a(-2)a(1)+2a(-1)a(0)\right]\Delta t^2}{4\varepsilon\mu\Delta y^2}\\
&J_j^e=-\frac{\left[2a(-2)a(2)+2a(-1)a(1)+a^2(0)\right]\Delta t^2}{4\varepsilon\mu\Delta y^2}\\
&H_j^e=-\frac{\left[2a(-1)a(2)+2a(0)a(1)\right]\Delta t^2}{4\varepsilon\mu\Delta y^2}\\
&I_j^e=-\frac{\left[2a(0)a(2)+a^2(1)\right]\Delta t^2}{4\varepsilon\mu\Delta y^2}\\
&J_j^e=-\frac{2a(1)a(2)\Delta t^2}{4\varepsilon\mu\Delta y^2},\ K_j^e=-\frac{a^2(2)\Delta t^2}{4\varepsilon\mu\Delta y^2}
\end{aligned}\right\}. \tag{10}$$

The Eq. (9) can be written in a matrix form as follows:

$$\mathbf{AX}=\mathbf{Y}, \tag{11}$$

where the coefficients matrix is as follows:

$$\mathbf{A}=\begin{bmatrix}
\mathbf{a}_1 & \mathbf{b}_1 & 0 & \cdots & 0 & \mathbf{t}\\
\mathbf{c}_2 & \mathbf{a}_2 & \mathbf{b}_2 & \cdots & 0 & 0\\
0 & \mathbf{c}_3 & \mathbf{a}_3 & \mathbf{b}_3 & \cdots & 0\\
\vdots & 0 & \ddots & \ddots & \ddots & \vdots\\
0 & \vdots & \cdots & \mathbf{c}_{n-1} & \mathbf{a}_{n-1} & \mathbf{b}_{n-1}\\
\mathbf{s} & 0 & 0 & \cdots & \mathbf{c}_n & \mathbf{a}_n
\end{bmatrix}. \tag{12}$$

Matrix $\mathbf{A}$ is a block periodic tri-diagonal matrix, and $\mathbf{a}_i$, $\mathbf{b}_i$, $\mathbf{c}_i$, $\mathbf{t}$, $\mathbf{s}$ are all m order square matrices. And the form of coefficient matrix $\mathbf{A}$ in Eq. (11) can be written as Eq. (12). In this work, the PS-ADI-MRTD equations are obtained based on the D2 wavelet [14]-[16], and $m=5$. The elements of matrices $\mathbf{a}_i$, $\mathbf{b}_i$, $\mathbf{c}_i$, $\mathbf{t}$ and $\mathbf{s}$ are as follows:

$$\mathbf{a}_1=\begin{bmatrix}
F_1^e & G_1^e & H_1^e & I_1^e & J_1^e\\
E_2^e & F_2^e & G_2^e & H_2^e & I_2^e\\
D_3^e & E_3^e & F_3^e & G_3^e & H_3^e\\
C_4^e & D_4^e & E_4^e & F_4^e & G_4^e\\
B_5^e & C_5^e & D_5^e & E_5^e & F_5^e
\end{bmatrix}, \tag{13}$$

$$\mathbf{b}_1=\begin{bmatrix}
K_1^e & 0 & 0 & 0 & 0\\
J_2^e & K_2^e & 0 & 0 & 0\\
I_3^e & J_3^e & K_3^e & 0 & 0\\
H_4^e & I_4^e & J_4^e & K_4^e & 0\\
G_5^e & H_5^e & I_5^e & J_5^e & K_5^e
\end{bmatrix}, \tag{14}$$

$$\mathbf{c}_2=\begin{bmatrix}
A_6^e & B_6^e & C_6^e & D_6^e & E_6^e\\
0 & A_7^e & B_7^e & C_7^e & D_7^e\\
0 & 0 & A_8^e & B_8^e & C_8^e\\
0 & 0 & 0 & A_9^e & B_9^e\\
0 & 0 & 0 & 0 & A_{10}^e
\end{bmatrix}, \tag{15}$$

$$\mathbf{t}=\begin{bmatrix}
A_1^e & B_1^e & C_1^e & D_1^e & E_1^e\\
0 & A_2^e & B_2^e & C_2^e & D_2^e\\
0 & 0 & A_3^e & B_3^e & C_3^e\\
0 & 0 & 0 & A_4^e & B_4^e\\
0 & 0 & 0 & 0 & A_5^e
\end{bmatrix}\exp\left(-jk_yT_y\right), \tag{16}$$

$$\mathbf{s}=\begin{bmatrix}
K_{n-4}^e & 0 & 0 & 0 & 0\\
J_{n-3}^e & K_{n-3}^e & 0 & 0 & 0\\
I_{n-2}^e & J_{n-2}^e & K_{n-2}^e & 0 & 0\\
H_{n-1}^e & I_{n-1}^e & J_{n-1}^e & K_{n-1}^e & 0\\
G_n^e & H_n^e & I_n^e & J_n^e & K_n^e
\end{bmatrix}\exp\left(jk_yT_y\right). \tag{17}$$

It is defined that $\mathbf{p}_1$, $\mathbf{q}_1$ are m order square matrices, $\mathbf{q}_n=\mathbf{p}_1^{-1}\mathbf{t}$, $\mathbf{p}_n=\mathbf{s}\mathbf{q}_1^{-1}$, and $\mathbf{p}=\begin{bmatrix}\mathbf{p}_1 & 0 & \cdots & 0 & \mathbf{p}_n\end{bmatrix}^{\mathrm{T}}$, $\mathbf{q}=\begin{bmatrix}\mathbf{q}_1 & 0 & \cdots & 0 & \mathbf{q}_n\end{bmatrix}^{\mathrm{T}}$, matrix $\mathbf{A}$ can be written as $\mathbf{A}=\mathbf{B}+\mathbf{p}\mathbf{q}^{\mathrm{T}}$, where:

$$\mathbf{B}=\begin{bmatrix}
\mathbf{a}_1-\mathbf{p}_1\mathbf{q}_1 & \mathbf{b}_1 & 0 & \cdots & 0 & 0\\
\mathbf{c}_2 & \mathbf{a}_2 & \mathbf{b}_2 & \cdots & 0 & 0\\
0 & \mathbf{c}_3 & \mathbf{a}_3 & \mathbf{b}_3 & \cdots & 0\\
\vdots & 0 & \ddots & \ddots & \ddots & \vdots\\
0 & \vdots & \cdots & \mathbf{c}_{n-1} & \mathbf{a}_{n-1} & \mathbf{b}_{n-1}\\
\mathbf{s} & 0 & 0 & \cdots & \mathbf{c}_n & \mathbf{a}_n-\mathbf{p}_n\mathbf{q}_n
\end{bmatrix}. \tag{18}$$

Following the Sherman-Morrison-Woodbury formula, we can get [17]:

$$\mathbf{A}^{-1}=\left(\mathbf{B}+\mathbf{p}\mathbf{q}^{\mathrm{T}}\right)^{-1}=\mathbf{B}^{-1}-\mathbf{B}^{-1}\mathbf{p}\left(\mathbf{I}_m+\mathbf{q}^{\mathrm{T}}\mathbf{B}^{-1}\mathbf{p}\right)^{-1}\mathbf{q}^{\mathrm{T}}\mathbf{B}^{-1}. \tag{19}$$

Suppose that matrix $\mathbf{B}$ is invertible and then the necessary and sufficient condition for matrix $\mathbf{A}$ to be invertible is that the $\mathbf{I}_m+\mathbf{q}^{\mathrm{T}}\mathbf{B}^{-1}\mathbf{p}$ is invertible. Finally, $\mathbf{A}^{-1}$ can be solved as follows:

$$\mathbf{A}^{-1}=\left(\mathbf{c}_{ij}\right)_{n\times n},\ \mathbf{c}_{ij}=\begin{cases}\mathbf{g}_i\mathbf{h}_j-\boldsymbol{\psi}_i\boldsymbol{\zeta}_j, & i\le j\\ \mathbf{x}_i\mathbf{y}_j-\boldsymbol{\psi}_i\boldsymbol{\zeta}_j, & i>j\end{cases}. \tag{20}$$

And $\mathbf{c}_{ij}$ is calculated as follows. For the given invertible matrices $\mathbf{p}_1$ and $\mathbf{q}_1$, where $\mathbf{q}_n = \mathbf{p}_1^{-1}\mathbf{t}$, $\mathbf{p}_n = \mathbf{s}\mathbf{q}_1^{-1}$, one can have:

$$\mathbf{u}_1 = \mathbf{a}_1 - \mathbf{p}_1\mathbf{q}_1$$
$$\mathbf{l}_{i-1} = \mathbf{c}_i\mathbf{u}_{i-1}^{-1},\ \mathbf{u}_i = \mathbf{a}_i - \mathbf{l}_{i-1}\mathbf{b}_{i-1}\ (i = 2,3,\cdots,n-1)$$
$$\mathbf{u}_n = \mathbf{a}_n - \mathbf{p}_n\mathbf{q}_n - \mathbf{l}_{n-1}\mathbf{b}_{n-1}$$
$$\boldsymbol{\alpha}_n = \mathbf{a}_n - \mathbf{p}_n\mathbf{q}_n,\ \boldsymbol{\beta}_i = \boldsymbol{\alpha}_{i+1}^{-1}\mathbf{c}_{i+1},$$
$$\boldsymbol{\alpha}_i = \mathbf{a}_i - \mathbf{b}_i\boldsymbol{\beta}_i\ (i = n-1, n-2,\cdots,1).$$

Defining that $\mathbf{g}_1 = \mathbf{I}_m$, $\mathbf{x}_1 = \mathbf{I}_m$, one can have:

$$\mathbf{h}_1 = \boldsymbol{\alpha}_i^{-1},\ \mathbf{h}_i = -\mathbf{b}_{i-1}\mathbf{h}_{i-1}\boldsymbol{\alpha}_i^{-1}\ (i = 2,3,\cdots,n)$$
$$\mathbf{g}_n = (\mathbf{u}_n\mathbf{h}_n)^{-1},\ \mathbf{g}_i = -\mathbf{b}_i\mathbf{g}_{i+1}\mathbf{u}_i^{-1}\ (i = n-1, n-2,\cdots,2)$$
$$\mathbf{y}_1 = \boldsymbol{\alpha}_1^{-1},\ \mathbf{y}_i = -\boldsymbol{\beta}_{i-1}\mathbf{y}_{i-1}\ (i = 2,3,\cdots,n)$$
$$\mathbf{x}_n = (\mathbf{u}_n\mathbf{h}_n)^{-1},\ \mathbf{x}_i = -\mathbf{l}_i\mathbf{x}_{i+1}\ (i = n-1, n-2,\cdots,2)$$
$$\boldsymbol{\xi} = \mathbf{I}_m + (\mathbf{q}_1\mathbf{g}_1\mathbf{h}_1 + \mathbf{q}_n\mathbf{y}_n\mathbf{x}_1)\mathbf{p}_1 + (\mathbf{q}_1\mathbf{g}_1\mathbf{h}_n + \mathbf{q}_n\mathbf{y}_n\mathbf{x}_n)\mathbf{p}_n$$
$$\boldsymbol{\psi} = \boldsymbol{\xi}^{-1}(\mathbf{p}_1\mathbf{x}_1\mathbf{y} + \mathbf{p}_n\mathbf{y}_n\mathbf{g}),\ \boldsymbol{\zeta} = \mathbf{q}_1\mathbf{g}_1\mathbf{h}^{\mathrm{T}} + \mathbf{q}_n\mathbf{y}_n\mathbf{x}^{\mathrm{T}}$$
$$\mathbf{c}_{ij} = \begin{cases} \mathbf{g}_i\mathbf{h}_j - \boldsymbol{\psi}_i\boldsymbol{\zeta}_j, & i \le j \\ \mathbf{x}_i\mathbf{y}_j - \boldsymbol{\psi}_i\boldsymbol{\zeta}_j, & i > j \end{cases}.$$

The TF/SF boundary and the absorbing boundary condition (ABC) of the PS-ADI-MRTD algorithm are similar to that of the traditional MRTD algorithm.

III. HANDLIING OF THE PERIODIC BOUNDARY CONDITION

For a better understanding of this paper, Fig. 2 shows a top view of a unit in a periodic structure, where T_x and T_y are the cycle lengths along the *x*- and *y*-direction, respectively, Nx_{F}, Nx_{L} and Ny_{F}, Ny_{L} are the first and last grid points along the *x*- and *y*-direction in the computational domain, respectively.

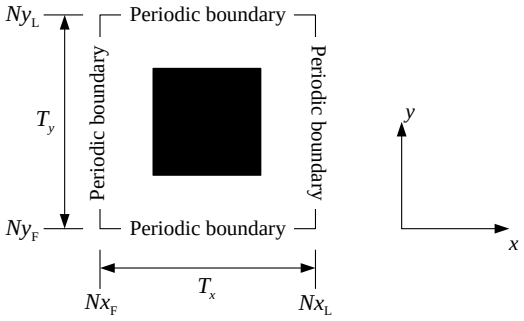

Fig. 2. Schematic diagram of the periodic structure unit.

Taking the electric fields as example, the periodic boundary condition of the MRTD can be expressed as follows:

$$E_x^n\left(i+\tfrac{1}{2}, Ny_{\mathrm{F}} \pm l, k\right) = E_x^n\left(i+\tfrac{1}{2}, Ny_{\mathrm{L}} \pm l, k\right)\exp\left(\mathrm{j}k_y T_y\right), \quad (21)$$
$$E_y^n\left(Nx_{\mathrm{F}} \pm l, j+\tfrac{1}{2}, k\right) = E_y^n\left(Nx_{\mathrm{L}} \pm l, j+\tfrac{1}{2}, k\right)\exp\left(\mathrm{j}k_x T_x\right), \quad (22)$$
$$E_z^n\left(i, Ny_{\mathrm{F}} \pm l, k+\tfrac{1}{2}\right) = E_z^n\left(i, Ny_{\mathrm{L}} \pm l, k+\tfrac{1}{2}\right)\exp\left(\mathrm{j}k_y T_y\right), \quad (23)$$
$$E_z^n\left(Nx_{\mathrm{F}} \pm l, j, k+\tfrac{1}{2}\right) = E_z^n\left(Nx_{\mathrm{L}} \pm l, j, k+\tfrac{1}{2}\right)\exp\left(\mathrm{j}k_x T_x\right). \quad (24)$$

The other set of equations for **H** can be obtained by duality. Where $l = 0,\ 1,\ 2\cdots$, it should be noted that the *l* is an effective support size for the MRTD basis function.

IV. NUMERICAL RESULTS

A. Scattering analysis of thin metal square array

In this section, a thin square metal plate array is calculated. As shown in Fig. 1, the edge length of a square metal plate is 0.5 cm, and the periodic unit size is $1\mathrm{cm}\times 1\mathrm{cm}$. The space is discretized by a mesh $\Delta x = \Delta y = \Delta z = \Delta = 0.05$ cm, the time step is $\Delta t_{\mathrm{CFL}} = \Delta / 3c$, and $\mathrm{CFLN} = \Delta t / \Delta t_{\mathrm{CFL}}$, where Δt_{CFL} is the time step limit defined by the stability condition of the traditional MRTD. $\mathrm{CFLN} = 3$ is used for the PS-ADI-MRTD method. The computational domain along the *z*-axis is truncated with absorbing boundary. The excitation is a TE wave with constant transverse wave-number (CTW) and the wave vector is on the *x*-*z* plane with $k_y = 0$. Therefore, the time domain expressions of the incident electric and magnetic fields can be expressed as follows:

$$E_y^{CTW} = \exp(-jk_x x) \times F^{-1}\left[\exp(jk_z(z-z_0))\exp(-\frac{k_0^2}{\sigma^2})\exp(-jt_0k_0c)\right], \quad (25)$$

$$H_x^{CTW} = \frac{1}{\eta_0}\exp(-jk_x x) \times F^{-1}\left[\exp(jk_z(z-z_0))\frac{k_z}{k_0}\exp(-\frac{k_0^2}{\sigma^2})\exp(-jt_0k_0c)\right], \quad (26)$$

where k_x denotes transverse wave-numbers, which are assumed to be constant numbers (independent of frequency). k_z is the normal wave-number, $k_0 = 2\pi f / c$. η_0 is the impedance of free space. The term $\exp(-k_0^2/\sigma^2)$ corresponds to a Gaussian pulse used to limit the bandwidth of the incident wave, and $\sigma = 950$. F^{-1} denotes the inverse Fourier transform. The frequency range here is from 1.0 GHz to 40GHz, then the k_x range is from 0.0 to 838rad/m.

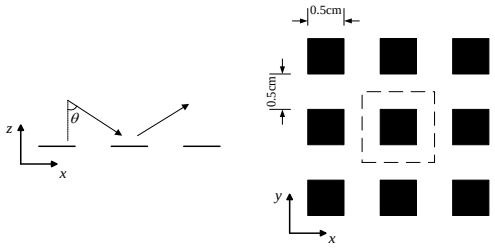

Fig. 1. Thin square metal sheet array.

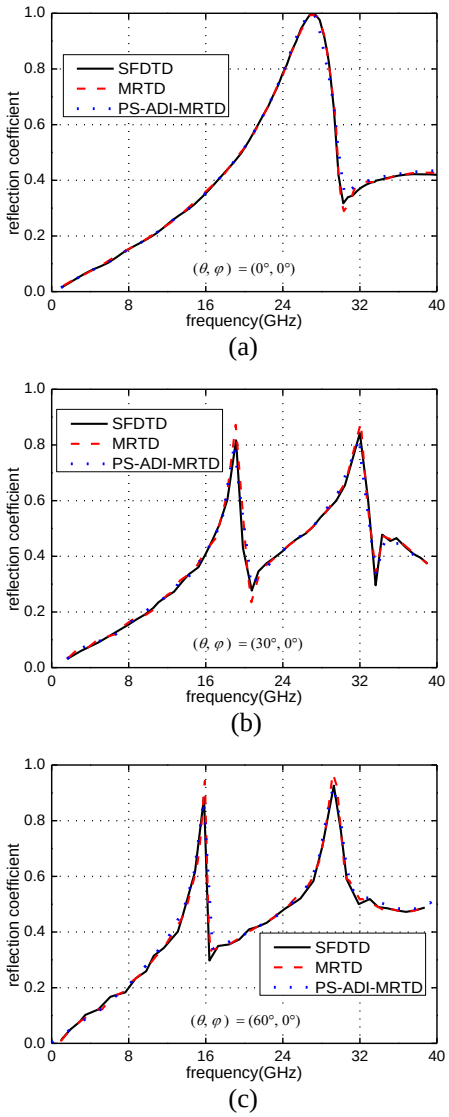

Fig. 2. The reflection coefficients with different incident angles.

Figure 2 shows the calculated reflection coefficients versus frequencies at different incident angles. As can be seen from Fig. 2, the numerical results of the proposed method are in good agreement with that of the MRTD and SFDTD, which verifies the accuracy of the PS-ADI-MRTD method. In addition, as shown in Table 1, numerical results also validate that although the PS-ADI-MRTD method uses more memory, it can save computing time by more than 26% compared with the traditional SFDTD and MRTD.

Table 1: CPU time and memory for different schemes

Schemes	CPU Time/s	CPU Memory/MB
SFDTD	3563.25	8.10
MRTD	1347.56	2.94
PS-ADI-MRTD	973.53	4.31

B. Application in frequency selective surface analysis

Frequency selective surface (FSS) is a kind of periodic structure which is widely used. It is generally composed of a certain number of passive resonant elements arranged in a specific way. Its main feature is that it can filter electromagnetic waves at different frequencies, incidence angles and polarization states. Two kinds of common FSS structures are periodically arranged sheet metal (patch type) and periodically opened sheet metal (aperture type). Generally speaking, in a certain frequency band near the resonance frequency, the former exhibits total reflection, while the latter exhibits total transmission [18]. In this section, the scattering characteristics in frequency domain are analyzed for the two types of FSS structures.

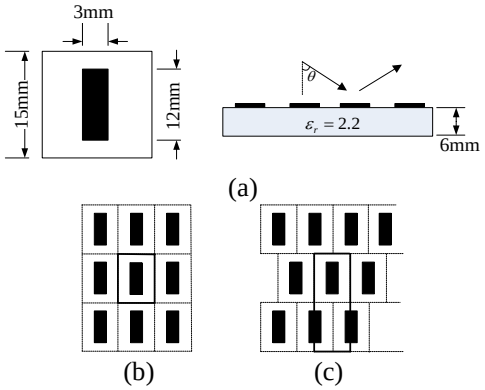

Fig. 3. Patch FSS structure and two array modes.

Figure 3 (a) is a periodic unit of a patch-type FSS structure and its placement on the substrate medium (black part is metal). The relative conductivity of the medium is $\varepsilon_r = 2.2$ and the thickness is 6 mm. Figure 3 (b) and Fig. 3 (c) are two kinds of array modes of FSS. The thickened wireframes in the figure are periodic units in two cases respectively. The setting of the constant transverse incident wave is also the same as that in Section III.A.

Figure 4 is the calculation result of two arrays under vertical incidence. It can be seen that the translation of the structure results in a slight shift of the reflection characteristic curve to the high frequency. The resonance frequencies before and after the translation are 9.5 GHz and 9.7 GHz respectively, and the second resonance frequency point appears in the array arrangement mode (b) at about 16.5 GHz.

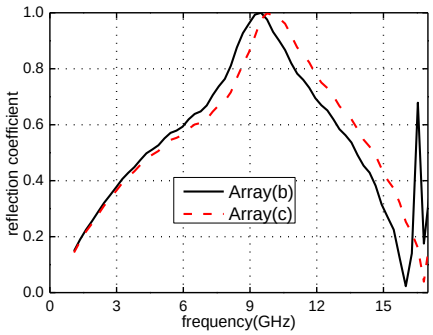

Fig. 4. Frequency characteristics of two array modes in vertical incidence.

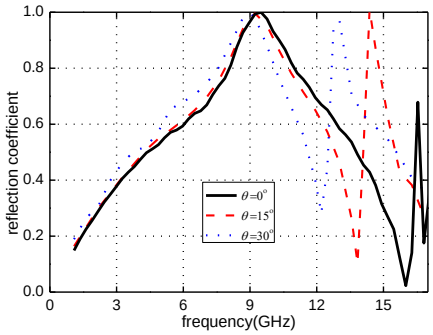

Fig. 5. Frequency characteristics of array mode (b) at different incidence angles.

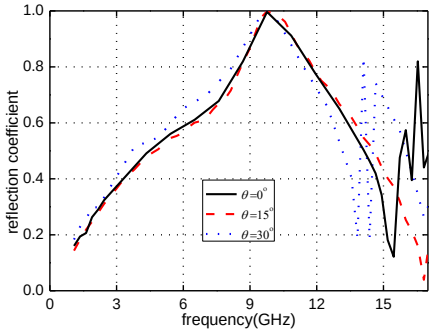

Fig. 6. Frequency characteristics of array mode (c) at different incidence angles.

Figure 5 and Fig. 6 show the results of two array modes when the incidence angle is 0°, 15° and 30°, respectively. It can be seen that the variation law of the two graphs is the same, and the reflection characteristic curve moves to the low frequency end with the increase of the incident angle. The first resonance frequency point appearing under the three incident angles has little difference, and the characteristic curve before the frequency point is also similar. As shown in Fig. 5, the second resonance frequencies of the array arrangement (b) at 15 and 30 degrees are 14.4 GHz and 13 GHz, respectively. From Fig. 6, it can be seen that the second and third resonance frequencies appear in the calculated frequency band after the array translation, such as the two consecutive resonance frequencies of 14 GHz and 14.6 GHz at the incident angle of 30 degrees, respectively.

Using the same method, we also calculated the frequency domain scattering characteristics of the aperture-type FSS structure shown in Fig. 7.

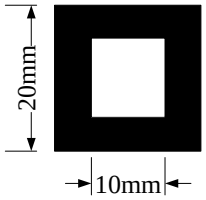

Fig. 7. Periodic cell of aperture-type FSS.

The calculated results at incident angles 0 degrees and 30 degrees are shown in Fig. 8 (a) and Fig. 8 (b) respectively. It can be seen that the resonant frequency point appears at about 13.8 GHz at vertical incidence, when the reflectivity is near zero and the corresponding transmittance is 1, which is consistent with the full transmission characteristics of the aperture FSS discussed above. When the incident angle increases, the resonant frequency is about 14.3GHz, and the reflectivity is about 0.48. It can also be seen from the figure that with the further increase of frequency, the frequency reflection characteristics of the structure are more complex.

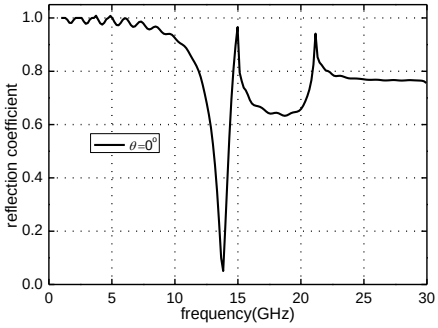

(a)

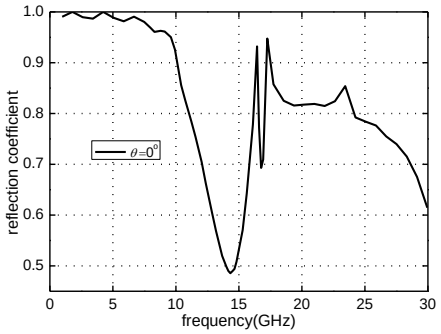

(b)

Fig. 8. Frequency characteristics of the aperture-type FSS.

V. CONCLUSION

In this paper, the spectral technique is applied to ADI-MRTD method for periodic structure calculation, and the PS-ADI-MRTD method is obtained. The inverse process of block periodic tridiagonal matrix is introduced and the numerical results verify the effectiveness and efficiency of the proposed PS-ADI-MRTD method. In the calculation case, the CPU time saveing is about 26%. Moreover, we apply this algorithm to analyze the frequency domain scattering characteristics of FSS and obtain the expected results, which further confirms the effectiveness of PS-ADI-MRTD algorithm.

REFERENCES

[1] M. Krumpholz and L. P. B. Katehi, "New prospects for time domain analysis," *IEEE Microwave Guid. Wave Lett.*, vol. 5, no.11, pp. 382-384, Dec. 1995.

[2] M. Krumpholz and L. P. B. Katehi, "MRTD: New time-domain schemes based on multiresolution analysis," *IEEE Trans. Microwave Theory Tech.*, vol. 44, no. 4, pp. 555-561, Apr. 1996.

[3] Y. W. Liu, Y. W. Chen, P. Zhang, and X. Xu, "Implementation and application of the spherical MRTD algorithm," *Progress In Electromagnetics Research*, vol. 139, pp. 577-597, 2013.

[4] Y. W. Liu, Y. W. Chen, and P. Zhang, "Parallel implementation and application of the MRTD with an efficient CFS–PML," *Progress in Electromagnetics Research*, vol. 143, pp. 223-242, 2013.

[5] P. Zhang, Y. W. Liu, S. Qiu, and B. Yang "CPML and quasi-CPML for cylindrical MRTD method," *Progress In Electromagnetics Research B*, vol. 61, pp. 17-30, 2014.

[6] C. Zhizhang and J. Zhang, "An unconditionally stable 3-D ADI-MRTD method free of the CFL stability condition," *IEEE Microwave and Wireless Components Letters*, vol. 11, no. 8, pp. 349-351, 2001.

[7] X. Dardenne and C. Craeye, "Method of moments simulation of infinitely periodic structures combining metal with connected dielectric objects," *IEEE Transactions on Antennas and Propagation*, vol. 56, no. 8, pp. 2372-2380, 2008.

[8] L. E. R. Petersson and J.-M. Jin, "A two-dimensional time-domain finite element formulation for periodic structures," *IEEE Transactions on Antennas and Propagation*, vol. 54, no. 1, pp. 12-19, 2005.

[9] S. Wang, J. Chen, and P. Ruchhoeft, "An ADI-FDTD method for periodic structures," *IEEE Transactions on Antennas and Propagation*, vol. 53, pp. 2343-2346, 2005.

[10] G. Singh, E. L. Tan, and Z. N. Chen, "Efficient complex envelope ADI-FDTD method for the analysis of anisotropic photonic crystals," *IEEE Photonics Technology Letters*, vol. 23, pp. 801-803, 2011.

[11] A. Amir and R. S. Yahya, "Spectral FDTD: A novel technique for the analysis of oblique incident plane wave on periodic structures," *IEEE Transactions on Antennas and Propagation*, vol. 54, no. 6, pp. 1818-1825, 2006.

[12] F. Yang, A. Elsherbeni, and J. Chen, "A hybrid spectral-FDTD/ARMA method for periodic structure analysis," *IEEE Antennas and Propagation Society International Symposium*, pp. 3720-3723, 2007.

[13] Y. F. Mao, B. Chen, H. Q. Liu, J. L. Xia ,and J. Z. Tang, "A hybrid implicit-explicit spectral FDTD scheme for oblique incidence problems on periodic structures," *Progress In Electromagnetics Research*, vol. 128, pp. 153-170, 2012.

[14] Y. W. Cheong, Y. M. Lee, K. H. Ra, J. G. Kang, and C. C. Shin, "Wavelet-Galerkin scheme of time-dependent inhomogeneous electromagnetic problems," *IEEE Microwave Guid, Wave Lett.*, vol. 9, no. 8, pp. 297-299, Aug. 1999.

[15] M. Fujii and W. J. R. Hoefer, "Dispersion of time domain wavelet Galerkin method based on Daubechies' compactly supported scaling functions with three and four vanishing moments," *IEEE Microwave Guid. Wave Lett.*, vol. 10, no. 4 pp. 125-127, Apr. 2000.

[16] I. Daubechies, *Ten Lectures on Wavelets*. SIAM, Philadelphia, PA, 1992.

[17] Y. Du, Q. Lu, and Z. Xu, "New algorithm for inversing block periodic tridiagonal matrices," *Computer Engineering and Applications*, vol. 48, no. 17, pp. 41-43, 2012.

[18] Y. Rahmat-Samii and H. Mosallaei, "Electromagnetic band-gap structures: Classsification, characterization and applications," *IEE-ICAP Symposium, Manchester, United Kingdom*, pp. 560-564, Apr. 17-20, 2001.